IJMMM International Journal of Minerals, Metallurgy and Materials 矿物冶金与材料学报（英文版）

Titanium dioxide-graphene composite electrochemical sensor for detection of hexavalent chromium

Natpichan Pienutsa, Krittamet Yannawibut, Jetthana Phattharaphongmanee, Oukrit Thonganantakul, and Sira Srinives

Cite this article as:
Natpichan Pienutsa, Krittamet Yannawibut, Jetthana Phattharaphongmanee, Oukrit Thonganantakul, and Sira Srinives, Titanium dioxide-graphene composite electrochemical sensor for detection of hexavalent chromium, *Int. J. Miner. Metall. Mater.*, 29(2022), No. 3, pp. 529-535. https://doi.org/10.1007/s12613-021-2338-7

View the article online at SpringerLink or IJMMM Webpage.

International Journal of Minerals, Metallurgy and Materials
Volume 29, Number 3, March 2022, Page 529
https://doi.org/10.1007/s12613-021-2338-7

Titanium dioxide-graphene composite electrochemical sensor for detection of hexavalent chromium

Natpichan Pienutsa, *Krittamet Yannawibut*, *Jetthana Phattharaphongmanee*, *Oukrit Thonganantakul*, *and Sira Srinives*✉

Nanocomposite Engineering Laboratory (NanoCEN), Department of Chemical Engineering, Faculty of Engineering, Mahidol University, 25/25 Puttamonthon, Nakhon Pathom, 73170, Thailand
(Received: 26 April 2021; revised: 25 June 2021; accepted: 10 August 2021)

Abstract: Hexavalent chromium (Cr(VI)) compound is useful to various industries but is toxic and carcinogenic. In this research work, we fabricate an amperometric sensor for the determination of Cr(VI), using a titanium dioxide (TiO_2)-reduced graphene oxide (rGO) composite as the sensing element. The composite was synthesized following sol−gel chemistry, yielding TiO_2 nanoparticles of ~50 nm in size, immobilized on chemically exfoliated rGO sheets. The composite was employed in a 3-electrode electrochemical cell and operated in an amperometric mode, exhibiting good responses to the 50 to 500 ppb Cr(VI). Our best result from pH 3 Mcilvane's buffer medium reveals the sensitivity of 9.12×10^{-4} ppb^{-1} and a detection limit of 6 ppb with no signal interference from 200 ppm Ca(II), 150 ppm Mg(II), and 50 ppb Pb(II). The excellent results of the TiO_2-rGO sensor can be attributed to synergic effects between TiO_2 and rGO, resulting from the presence of n-p heterojunctions and the formation of the TiO_2 nanoparticles on rGO.

Keywords: photocatalyst; electrochemical sensor; hexavalent chromium; graphene

1. Introduction

Chromium is a heavy metal commonly present in soil, groundwater, and surface water. Natural oxidative states of chromium include trivalent chromium (Cr(III)) and hexavalent chromium (Cr(VI)). While Cr(III) is generally regarded as harmless, Cr(VI) is known for its toxicity, genotoxicity, and carcinogenic properties [1−2]. Cr(VI) compounds are currently used in various industries, including steel production, leather tanning, and electroplating [2−5]. Wastewater from such industries is treated mainly via chemical treatment or bioremediation and discharged, following regulations enforced by the local government. The typical guideline from the US Environmental Protection Agency (EPA) limits 100 μg/L (~100 ppb) for total chromium concentration in drinking water. The term total chromium was used, considering possible back-and-forth conversion of Cr(VI) to Cr(III) in both the environment and the human body. The Cr(VI) presence still is the primary concern, and an electronic device with the ability for real-time monitoring of Cr(VI) at the desired concentration range is needed.

Several techniques are currently employed to determine Cr(VI) in water and utilize spectroscopy instruments, such as UV−Visible spectroscopy and atomic absorption spectroscopy [6]. However, these techniques rely heavily on trained personnel and massive lab equipment, inhibiting on-site and real-time monitoring. A good amount of effort has been invested in developing and improving Cr(VI) measurement. For example, Zazuoa *et al.* [7] immobilized the tributylphosphate ionophore, a Cr(VI) recognition molecule, on the ion-sensitive field-effect transistor (ISFET). The device exhibited a wide detection range of 10^{-5} to 0.5 M Cr(VI) but with cross-interference against lead and cadmium. Chen *et al.* [8] used graphene nanosheets as a graphene quantum dot with outstanding electrochemiluminescence (ECL) properties. The graphene was activated via electrochemistry and was chemically quenched in Cr(VI), creating an ECL signal. Korshoj *et al.* [9] fabricated an amperometric sensor based on electrocatalytic reactions between Cr(VI) and methylene blue. The group reported a detection limit (LOD) in the nM scale with no significant interference from other heavy metal ions. Despite such development, there is plenty of room for developing a fast and straightforward technique that can provide real-time measurement with high sensitivity and selectivity toward Cr(VI).

Titanium dioxide (TiO_2) is a well-known photocatalyst and is employed widely for environmental-related applications. Its popularity came from good photocatalytic reliability, chemical stability, and commercial availability. A few researchers also demonstrated use of TiO_2 in photocatalytic reduction of Cr(VI) to Cr(III) [10−11]. Major concerns exist over the TiO_2 photocatalyst regarding its wide energy band

✉ Corresponding author: Sira Srinives E-mail: sira.sri@mahidol.edu

gap and fast electron-hole recombination rate. The former restricts the uses of TiO_2 in the absence of ultraviolet light, while the latter reduces the material's photocatalytic performances.

Graphene is a two-dimensional nanostructure and an allotrope of carbon with high electrical conductivity, large surface-to-volume ratio, and high chemical stability. Since it was discovered, it has been demonstrated for a broad spectrum of applications, such as reinforcing material for polymer, supporting metal oxide-graphene catalysts, and as sensitive material for an electrochemical sensor [12−14]. Graphene can be synthesized following a chemical exfoliation method to be electrically insulating graphene oxide (GO), which contains functional groups, such as carboxyl, carbonyl, and hydroxyl. The functional groups can be partially removed by introducing the GO to a strong reducing agent, such as hydrazine or L-ascorbic acid, to create the semiconducting reduced graphene oxide (rGO). Combination of the TiO_2 and graphene creates the TiO_2-graphene composite, which functions as an excellent photocatalyst. The roles of the graphene here are to provide supporting material for the TiO_2 to immobilize on and yield the TiO_2-graphene interfaces. The interfaces house active radicals, such as oxygen anions and electrons, which can promote reactions. The interfaces also function as n-p heterojunctions, which help reduce the electron-hole recombination phenomenon [15].

In this work, we synthesized the TiO_2-rGO composite and utilized it as a working electrode for amperometric measurement of Cr(VI). The amperometric sensor showed excellent responses to Cr(VI) and was tested against different pH values and selected chemicals and metal ions. The TiO_2, rGO, and TiO_2-rGO composite samples were characterized via transmission electron microscope (TEM), Fourier transform infrared spectroscopy (FTIR), and UV−Vis for their physical, chemical, and optical properties, respectively.

2. Experimental

2.1. Materials

All chemical reagents were of analytical grade and used as received. Graphene flake (natural, 99.9%; metal basis; 10 mesh) was purchased from Alfa Aesar (USA), sulfuric acid (H_2SO_4; analytical reagents (AR) grade, 98%), Ethanol (AR grade, 99.9%) were purchased from RCl Labscan (Thailand). Titanium butoxide ($Ti(OCH_2CH_2CH_2CH_3)_4$, Reagent grade) and Disodium hydrogen phosphate (Na_2HPO_4, 99%) were purchased from Sigma-Aldrich Co., Ltd. Hydrogen peroxide (30wt% solution) was purchased from Merck (Germany). Citric acid ($C_6H_8O_7$, 99%), calcium chloride ($CaCl_2$, 99%), and magnesium chloride ($MgCl_2$, 99%) were purchased from Ajax FineChem (India). Lead(II) nitrate ($Pb(NO_3)_2$, 99%) was purchased from BDH Co., Ltd. All solutions were prepared using deionized (DI) water (Milli-Q water). Mcilvaine's buffer solutions were prepared at the desired pH by mixing 0.2 M disodium hydrogen phosphate and 0.1 M critic acid solutions.

2.2. Synthesis of GO and rGO

The graphene oxide (GO) was synthesized following a modified Hummer's method, proposed by Zhang *et al.* [16]. Briefly, natural graphite flakes of 2 g were mixed with sodium nitrate of 1 g in a concentrated sulfuric acid solution of 50 mL. 7.3 g of potassium permanganate was slowly added while the mixture was stirred below 4°C for 2 h. The mixture was raised to 35°C and stirred for another 2 h. DI water of 90 mL was poured in to dilute the viscous mixture, followed by the addition of hydrogen peroxide solution (7 mL of 30wt% H_2O_2 in 55 mL DI water). A brown slurry of GO was filtrated from the mixture using a vacuum filtration set with glass fiber microfilters (GF/C Whatman). The GO was rinsed several times with a sequence of hydrochloric acid solution (3vol% HCl in DI water) and DI water. The GO powder was heated at 60°C in an oven for 12 h and kept under desiccant for future use.

For the rGO synthesis, GO suspension was prepared by sonicating GO powder in DI water using an ultrasonic bath (0.25 mg/mL). L-ascorbic acid (reducing agent) was added to the mixture at 2.5 mg/mL, converting GO to rGO. The mixture was stirred for 24 h before the rGO powder was obtained via vacuum filtration. The rGO powder was dried at 90°C for 12 h and kept in a desiccator for future uses.

2.3. Synthesis of the TiO_2-rGO composite

The TiO_2-rGO composite was synthesized using a sol−gel method. The process started by suspending rGO in a 20 mL mixture of water and ethanol (1:1 in volume ratio) at a 5 mg/mL concentration, followed by a dropwise addition of titanium butoxide solution (2 mL titanium butoxide in 8 mL ethanol). The mixture was stirred for 1 h and further heated to 90°C to evaporate water and ethanol. The solid residual was calcined at 600°C for 1 h to obtain the TiO_2-rGO composite powder. The pristine TiO_2 nanoparticles were prepared in the same manner with no rGO powder.

2.4. Sample characterizations

The TiO_2-rGO and graphene samples were characterized for physical and chemical properties. The composite's physical morphology was observed using the transmission electron microscope (TEM; FEI TECNAI T20 G2) at an accelerating voltage of 200 kV and an electron beam energy of 100 keV. The UV−Vis spectra (T60 UV−Visible Spectrophotometer, PG Instruments) were obtained by scanning wavelengths in the range of 200−800 nm on the aqueous suspension of either TiO_2-rGO composite, rGO, or TiO_2 particles. Optical band gaps were determined from the Tauc's relation (Eq. (1)), the plot of light absorbance (A) and photon energy ($h\nu$), in which

$$(\alpha h\nu)^{1/n} = C(h\nu - E_g) \quad (1)$$

where $\alpha = 2.303A/t$, A is the light absorbance, t is the quartz cell thickness (1 cm), $h\nu$ is the photon energy (eV), $h\nu$ (eV) = 1240/[wavelength (nm)], C is the arbitrary constant, E_g is the

energy band gap (eV), n is the power factor of the transition mode ($n = 2$ for direct band gap energy).

The linear range of the plot of $(\alpha h\nu)^{1/n}$ versus $h\nu$ was extended to the abscissa to obtain the E_g value. The FTIR spectrophotometer (Nicolet 6700, Thermo Fisher Scientific) was operated in transmittance mode and wavenumber range of 400−4000 cm^{-1}. The rGO, TiO_2-rGO, and TiO_2 samples were also characterized by X-ray diffraction (Miniflex II, Rigaku) with the Cu K_α wavelength of 0.154 nm.

2.5. Fabrication of the TiO_2-rGO composite amperometric sensor

The glassy carbon electrode (GCE) was polished using 1, 0.3, and 0.05 µm alumina powder on separated pads of polishing cloth. The GCE was rinsed with water and ethanol before drying in a nitrogen stream. A suspension of 1 mg/mL TiO_2-rGO composite in DI water was cast on the GCE at 10 µL drop size to realize a mass to surface area of 5.65 µg/mm^2, creating a uniform composite film of TiO_2-rGO on the electrode. The rGO and TiO_2 sensors were produced in the same manner as the composite sensor, replacing the TiO_2-rGO with rGO and TiO_2, respectively.

2.6. Electrochemical experiments

All electrochemical experiments were performed on the electrochemistry workstation (CHI 1206B, CHI instrument). The GCE was employed as a working electrode (WE) in a 3-electrode electrochemical cell. The Ag/AgCl electrode and platinum wire were used as a reference electrode (RE) and a counter electrode (CE). In a cyclic voltammogram analysis (CV), scanning potential was applied in −1 to 1 V window at a scanning rate of 50 $mV \cdot s^{-1}$. In the amperometric sensing experiment, the TiO_2-rGO on GCE was operated under a constant potential of −0.4 V in Mcilvaines' buffers (pH 3, 4, or 5). Potassium dichromate ($K_2Cr_2O_7$) solution was added to the buffer to create 50 to 500 ppb Cr(VI) for amperometric sensing. A standard UV−Vis spectroscopy test, the method 7196A, was conducted to provide comparison measurements on the Cr(VI) concentrations. The selectivity of the sensor was investigated by testing the sensor against metal ions, including Cr(VI), Ca(II), Mg(II), and Pb(II).

The standard method 7196A is a popular procedure for the determination of Cr(VI), which relies on the light adsorption characteristics of the product from the reaction of Cr(VI) and diphenyl carbazide. In brief, 2 mL of diphenyl carbazide in acetone (5 mg/mL) was added to 95 mL of Cr(VI) solution in a 100 mL volumetric flask. The mixture was titrated to pH 2 ± 0.5 using sulfuric acid solution and diluted to 100 mL with DI water. Then, the light-absorbing spectra were generated using the UV−Visible spectrophotometer (T60 UV−Visible Spectrophotometer, PG Instruments) at 540 nm. The stock Cr(VI) solution was prepared by dissolving 141.1 mg of potassium dichromate to 1 L DI water, and the standard Cr(VI) solution was prepared by diluting the stock Cr(VI) solution to the desired Cr(VI) concentration.

3. Results and discussion

3.1. Sample characterizations

Physical morphology of the TiO_2-rGO was observed by the TEM (Fig. 1(a)), in which TiO_2 nanoparticles are ~50 nm in size and are distributed on the graphene sheet. The optical characteristic of the rGO, TiO_2 particles, and TiO_2-rGO composite were revealed via the UV−Vis spectra (Fig. 1(b)). The rGO exhibits a light absorption peak at ~230 nm and partially absorbs visible light, while the TiO_2 shows only a strong light absorption peak in the UV region. On the other hand, the TiO_2-rGO displays a broad absorption peak at 340 nm, covering UV and visible light regions. Optical band gap energies, obtained from the Tauc plot (inset in Fig. 1(b)), were determined as 2.2, 3.4, and 2.8 eV for the rGO, TiO_2, and TiO_2-rGO composite, respectively. The band gap energies here were comparable to those from the literature [6,17−18], and support our hypothesis that the TiO_2-rGO composite would yield enhanced photocatalytic performances.

Crystal structures of the TiO_2, rGO, and TiO_2-rGO composite were characterized by XRD. The TiO_2 (Fig. 1(c), middle line) exhibits X-ray diffraction peaks at 2θ of 26°, 38°, 48°, 56°, and 63°, which can be indicated to the 101, 004, 200, 106, and 215 planes of TiO_2 anatase [19]. The rGO reveals XRD diffraction peaks at 15° and 25°, which represent (001) and (002) planes of graphitic structures (Fig. 1(c), bottom line). The XRD spectra of the TiO_2-rGO composite (Fig. 1(c), top line) display a similar crystallographic pattern to that of the TiO_2 particles. The graphene diffraction peak does not appear in the composite spectra, which resulted from the relatively low diffraction intensity of the rGO [16].

The FTIR spectra of rGO (Fig. 1(d)) reveal the transmittance peak of hydroxyl stretching (−OH) at ~3400 cm^{-1}, which can be appointed to a water hydroxyl and a carboxylic hydroxyl group. Small peaks at ~3000 and 1400 cm^{-1} could be assigned to the methylene group (=C−H) and methyl group (−C−H) of the graphene's edges. The sharp peak at ~1727 cm^{-1} can be attributed to the carbonyl (−C=O) part of the carboxyl group (−COOH), while the other peak at ~1100 cm^{-1} represents the alkene group (−C=C−) of the graphene [16]. For the TiO_2 samples, the FTIR spectra exhibit a sharp peak of Ti−O−Ti vibration at 400−900 cm^{-1} [6] and a hydroxyl peak at ~3400 cm^{-1}. The TiO_2-rGO composite shows IR adsorption peaks for the carboxyl (~3400 cm^{-1}), carbonyl (~1700 cm^{-1}), and alkene groups (~1100 cm^{-1}). The broad peak at 400−900 cm^{-1} was either attributed to the vibration of the Ti−O−C bond or the Ti−O−Ti bond [6]. The broad peak here is evidence that TiO_2 nanoparticles may either chemically bond via Ti−O−C interactions or physically attach to the rGO sheet.

3.2. Electrochemical experiments

The CV curves (Fig. 2) present the electroactivity of the rGO, TiO_2, and TiO_2-rGO composite. The composite (Fig. 2(a)) exhibits an anodic current curve starting from −0.4 to

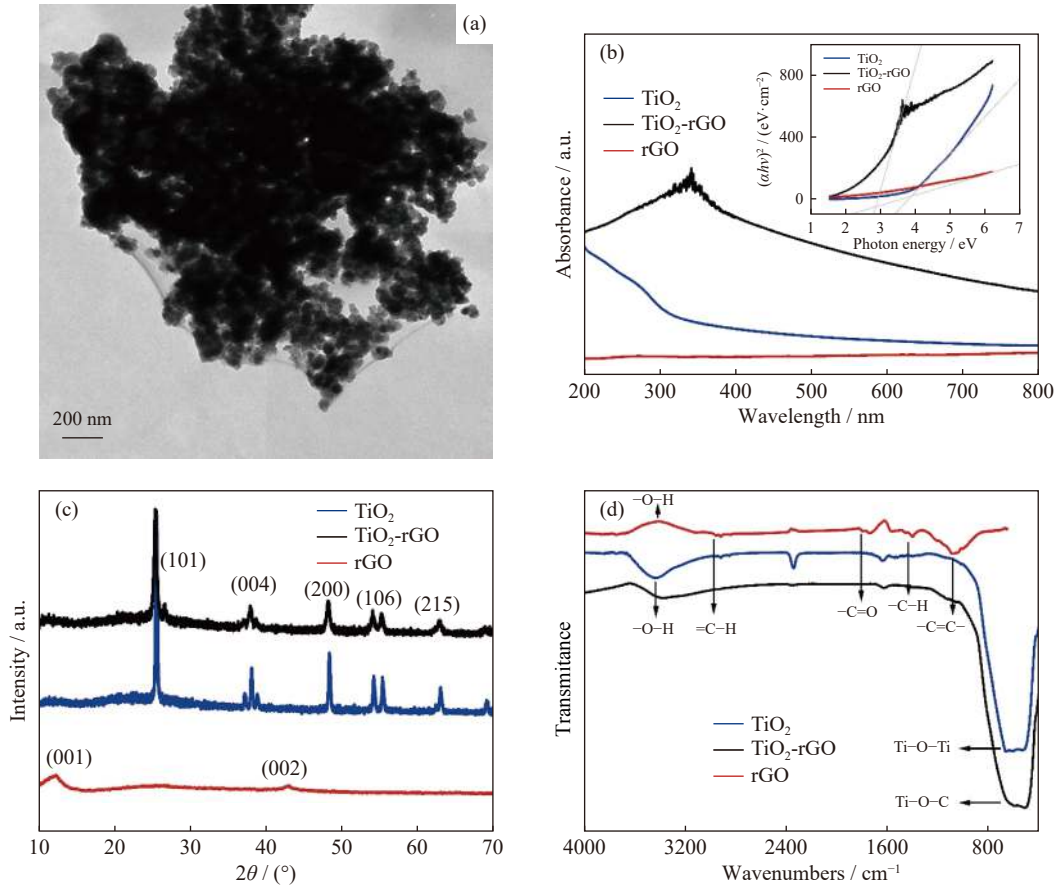

Fig. 1. (a) TEM image showing TiO_2 nanoparticles immobilized on rGO sheet; (b) UV−Vis spectra of TiO_2, TiO_2-rGO composite, and rGO and (inset) Tauc's plot exhibiting energy band gap on the abscissa; (c) XRD spectra of rGO, TiO_2-rGO, and TiO_2 samples, indicating presence of the anatase TiO_2; (d) FTIR spectra of TiO_2, TiO_2-rGO composite, and rGO samples.

−1.0 V, corresponding to the reduction of Cr(VI) to Cr(III). The result agreed well with data from Lee and his team [19], reporting the reduction potential for Cr(VI) in the range of −0.35 to −0.5 V. Reduction currents (Fig. 2(a) (Inset)) corresponding to the background medium of 0 and 500 ppb Cr(VI) are -2.03×10^{-5} and -2.50×10^{-5} A, respectively. On the other hand, the TiO_2 (Fig. 2(b)) and rGO (Fig. 2(b) (Inset)) showed no significant responses to the Cr(VI), which could be attributed to TiO_2 having low surface activity and rGO lacking affinity to Cr(VI) analyte.

CV analysis was also performed on the TiO_2-rGO composite to observe effects from the light source on the electrochemical activity of the composite. A mercury lamp (Phillips, 160 W) and a fluorescent lamp (Visible light, Phillips, 14 W) were used as the light source in a closed chamber. It is worth noting that the mercury lamp emits light in both UV and visible regions, while the fluorescent lamp emits light in the visible region. Normalized reduction currents were determined by dividing the reduction current at −0.4 V of 5 ppm Cr(VI) response with that of the 0 ppm (Background). The normalized reduction currents are 1.06, 1.21, and 1.23 in the dark, visible, and ultraviolet light sources, respectively. The TiO_2-

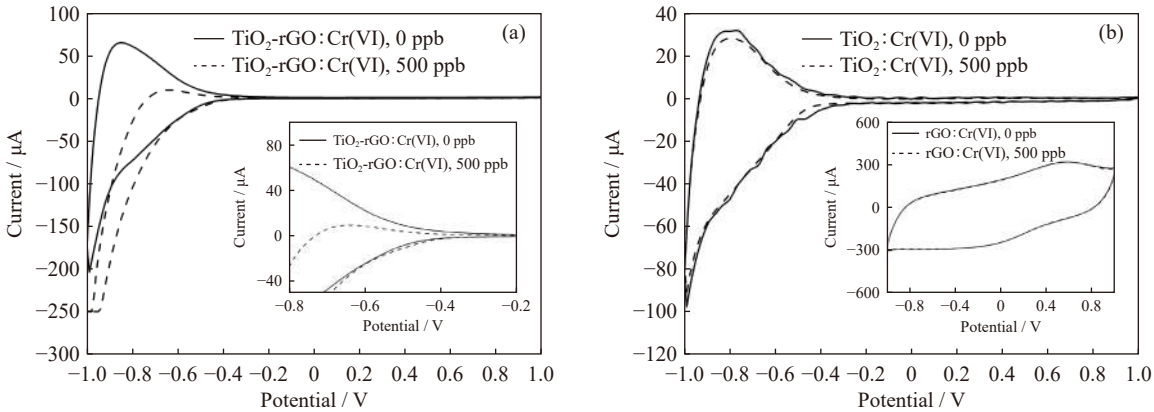

Fig. 2. (a) Cyclic voltammograms showing electroactivity of TiO_2-rGO as corresponding to Cr(VI), and (inset) zoom-in of the cyclic voltammograms; (b) cyclic voltammograms of TiO_2 and (inset) rGO samples as corresponding to Cr(VI).

rGO composite exhibits stronger electrochemical activity under UV light (Fig. 3(a)) compared to that of the visible light (Fig. 3(b)). The composite shows no response to the Cr(VI) when kept in the dark environment (Fig. 3(b) (Inset)) since the TiO_2 remains photocatalytically inactive in the dark environment [20].

The amperometric sensing of Cr(VI) was performed using TiO_2-rGO composite on GCE as the WE. The GCE (WE) was employed in the electrochemical cell along with CE and RE in a background medium of pH 3 McIlvaine buffer. The constant potential of −0.4 V was applied to the WE versus the RE in the amperometric mode, in which changes in electrochemical current were monitored as sensing responses (Fig. 4(a)). The electrochemical current rises as introduced to the Cr(VI), which indicates electron transfer from WE to active radicals in the medium. The TiO_2-rGO composite sensor provides much larger responses than those of the rGO sensor (Fig. 4(b)), stating involvement of the photocatalytic reaction to the reduction of Cr(VI) to Cr(III) [15]. Roles of the TiO_2 can be explained since the photoactivation on TiO_2 nanoparticles causes electrons to jump from the valence band to the conductive band and generates active electrons that reduce the Cr(VI) [19]. A calibration plot was generated by plotting a ratio of electrochemical current (I) as corresponding to a Cr(VI) concentration and baseline current (I_0) with the Cr(VI) concentration (Fig. 4(b)). In the buffer solution of pH 3, the composite sensor provided the linear response window of 50 to 500 ppb ($R^2 = 0.99$, $n = 5$), while its sensitivity was determined from the calibration plot's slope to be 9.12×10^{-4} ppb^{-1}. The detection limit was determined to be 6 ppb, relying on a signal-to-noise ratio of 3.

For the effect of medium pH, the amperometric sensing was performed in a buffer solution of pH 4 and 5 (Fig. 4(b)). The results stated strong dependence of sensing performances on the solution pH as the sensitivity to Cr(VI) was determined as 3.26×10^{-4} and 1.02×10^{-4} ppb^{-1} in the buffer solutions of pH 4 and 5, respectively. Higher sensitivity at lower pH solutions can be attributed to the equilibrium of chromate (CrO_4^{2-}) and dichromate ($Cr_2O_7^{2-}$) (Eq. (2)). The chromate form is the prime species in an alkali solution, while the dichromate is dominant in an acid solution [21]. The lower the pH, the more the dichromate species. The dichromate undergoes the electrooxidation reaction, yielding electrochemical current for the sensing signal (Eq. (3)), and produces trivalent chromium (Cr(III)) and water molecules.

$$2CrO_4^{2} + 2H^{+} \rightleftharpoons Cr_2O_7^{2} + H_2O \qquad (2)$$

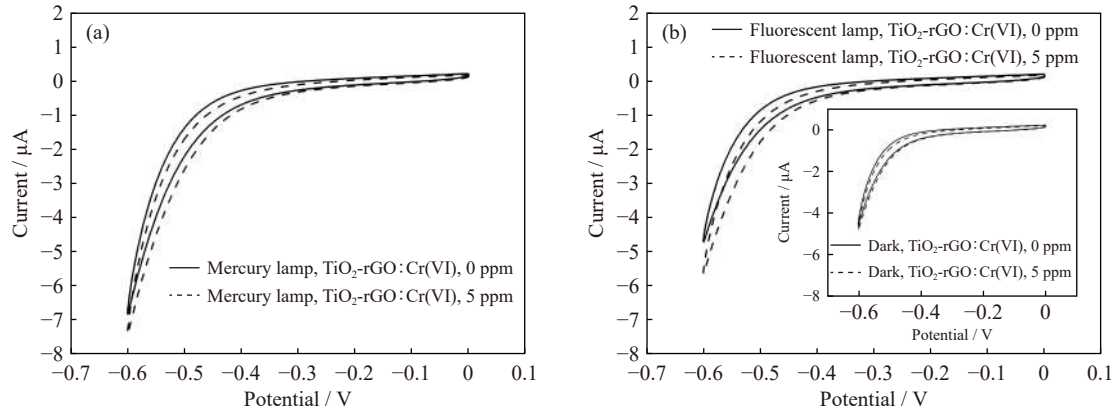

Fig. 3. (a) Cyclic voltammograms displaying electroactivity of TiO_2-rGO as corresponding to 5 ppm Cr(VI) in presence of mercury lamp; (b) Cyclic voltammograms of TiO_2-rGO showing response to 5 ppm Cr(VI) in presence of fluorescent lamp and (inset) in presence of dark environment.

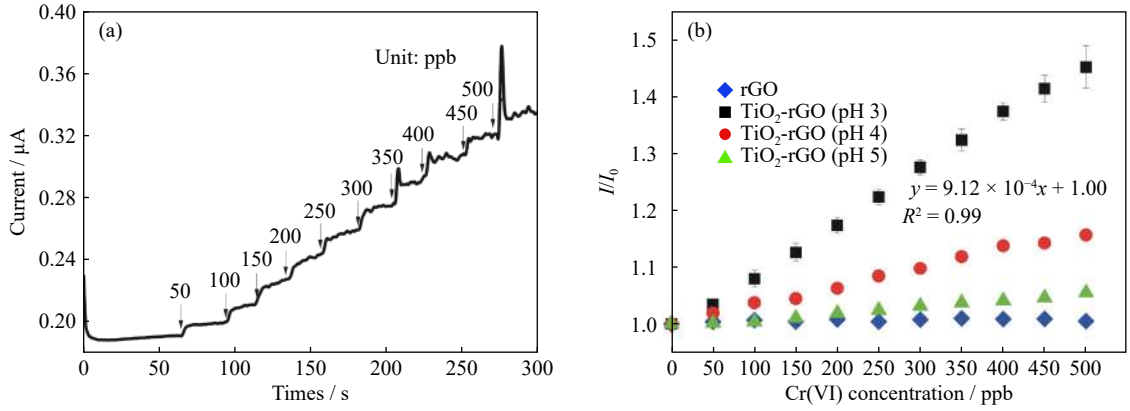

Fig. 4. (a) Amperometric sensing curve showing responses of TiO_2-rGO sensor to Cr(VI) in 50–500 ppb concentration window; (b) calibration plot of sensing responses versus Cr(VI) concentrations of rGO (pH 3), TiO_2-rGO (pH 3), TiO_2-rGO (pH 4), and TiO_2-rGO (pH 5).

$$Cr_2O_7^{2-} + 14H^+ + 6e^- \rightarrow 2Cr(III) + 7H_2O \quad (3)$$

3.3. Comparison of the sensor readout and the UV−Visible standard method

Sensing signals of the TiO_2-rGO provided readouts for Cr(VI) concentrations. The sensing readout values were compared to those from the UV−Vis Method 7196A, while the concentration values of the prepared solution were used as the standard. For the composite sensor, the deviations were determined to be 2.67%, 1.60%, and 1.71% (Fig. 5(a)), corresponding to the concentrations of 150, 250, and 350 ppb, respectively. For Method 7196A, the deviations of 0.67%, 0, and 0.57% were determined. Results from the sensor measurement and Method 7196A state that the composite-based amperometric sensor provides relatively lower accuracy than that of UV−Vis method. However, the composite sensor still is a valuable platform that yields fast readout for Cr(VI) concentrations and can be developed for a portable device.

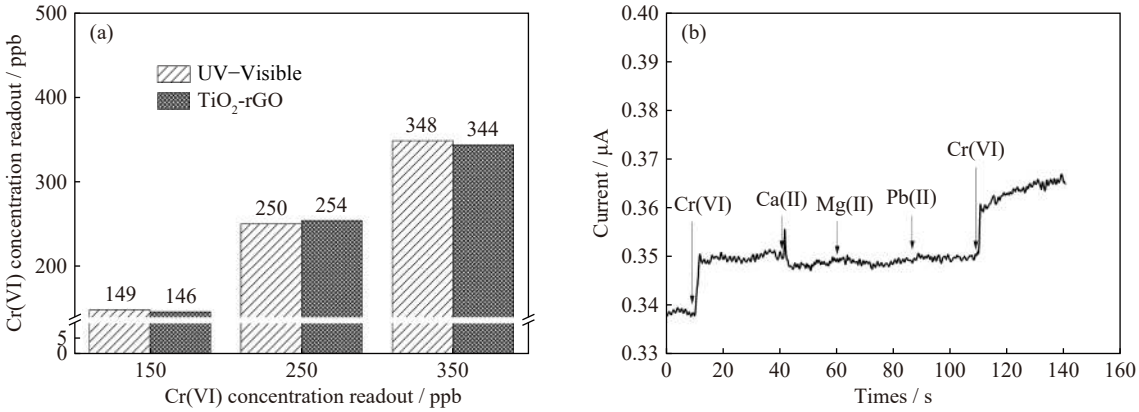

Fig. 5. (a) Bar charts exhibiting comparison of sensing responses from the TiO_2-rGO sensor and the UV−Vis Method 7196A; (b) amperometric sensing curve showing responses of the TiO_2-rGO sensor to 50 ppb Cr(VI), 200 ppm Ca(II), 150 ppm Mg(II), and 50 ppb Pb(II).

3.4. Interferences

The sensor was tested in pH 3 buffer solution against other chemicals, including 200 ppm calcium (Ca(II) from $CaCl_2$), 150 ppm magnesium (Mg(II) from $MgCl_2$), and 50 ppb lead (Pb(II) from $Pb(II)(NO_3)_2$) to demonstrate the practicality of the composite sensor. A certain concentration of a chemical was created by adding the stock solutions to the electrochemical cell. The sensor exhibited no significant response to the Ca(II), Mg(II), and Pb(II) in the concentration range that we tested (Fig. 5(b)), proving only a sensing signal to 50 ppb of Cr(VI).

4. Conclusion

We synthesized TiO_2-rGO composite using a sol−gel method that yields the anatase phase TiO_2 as the main crystallographic structure. The composite was coated on a glassy carbon working electrode and used in the amperometric sensor for Cr(VI) detection. The linear responses were observed upon exposing the sensor to 50−500 ppb of Cr(VI) while the limit of detection was determined to be 6 ppb (signal to noise ratio = 3) at pH 3. An increase in solution pH leads to a significant reduction in sensor response intensity. No significant responses were spotted during the introduction of Pb(II), Ca(II), and Mg(II) to the sensor. Results from the sensor were cross-checked with those from the standard method for Cr(VI) detection. The results showed a less than 2.54% deviation in Cr(VI) concentration readout.

Acknowledgements

Sira Srinives would like to convey his sincere gratitude to the Coordinating Center for Thai Government Science and Technology Scholarship Students (National Science and Technology Development Agency (NSTDA)), Mahidol University and the Faculty of Engineering, Mahidol University for their financial supports.

Conflict of Interest

All the authors declare that there is no conflict of interest.

References

[1] F. Xu, T. Ma, L. Zhou, Z.F. Hu, and L. Shi, Chromium isotopic fractionation during Cr(VI) reduction by Bacillus sp. under aerobic conditions, *Chemosphere*, 130(2015), p. 46.

[2] Y.S. Hedberg and C. Lidén, Chromium(III) and chromium(VI) release from leather during 8 months of simulated use, *Contact Dermat.*, 75(2016), No. 2, p. 82.

[3] B. Kim, S. Kim, and H. Kim, Effects of alloying elements (Cr, Mn) on corrosion properties of the high-strength steel in 3.5% NaCl solution, *Adv. Mater. Sci. Eng.*, 2018(2018), p. 1.

[4] J. Kotaś and Z. Stasicka, Chromium occurrence in the environment and methods of its speciation, *Environ. Pollut.*, 107(2000), No. 3, p. 263.

[5] K.K. Krishnani, S. Srinives, B.C. Mohapatra, V.M. Boddu, J.M. Hao, X. Meng, and A. Mulchandani, Hexavalent chromium removal mechanism using conducting polymers, *J. Hazard. Mater.*, 252-253(2013), p. 99.

[6] S.A. Miscoria, C. Jacq, T. Maeder, and R. Martín Negri, Screen-printed electrodes for electroanalytical sensing, of chro-

mium VI in strong acid media, *Sens. Actuators B*, 195(2014), p. 294.
[7] A. Zazoua, S. Zougar, R. Kherrat, M.H. Samar, N. Jaffrezic-Renault, A. Errachid, and A. Abbaci, Development of a hexavalent chromium ISFET sensor with a polymeric membrane including tributylphosphate, *Mater. Sci. Eng. C*, 26(2006), No. 2-3, p. 568.
[8] Y.M. Chen, Y.Q. Dong, H. Wu, C.Q. Chen, Y.W. Chi, and G.N. Chen, Electrochemiluminescence sensor for hexavalent chromium based on the graphene quantum dots/peroxodisulfate system, *Electrochim. Acta*, 151(2015), p. 552.
[9] L.E. Korshoj, A.J. Zaitouna, and R.Y. Lai, Methylene blue-mediated electrocatalytic detection of hexavalent chromium, *Anal. Chem.*, 87(2015), No. 5, p. 2560.
[10] Y. Ku and I.L. Jung, Photocatalytic reduction of Cr(VI) in aqueous solutions by UV irradiation with the presence of titanium dioxide, *Water Res.*, 35(2001), No. 1, p. 135.
[11] V. Loryuenyong, N. Jarunsak, T. Chuangchai, and A. Buasri, The photocatalytic reduction of hexavalent chromium by controllable mesoporous anatase TiO_2 nanoparticles, *Adv. Mater. Sci. Eng.*, 2014(2014), art. No. 348427.
[12] K. Chen, Z.L. Zhang, Y.M. Liang, and W. Liu, A graphene-based electrochemical sensor for rapid determination of phenols in water, *Sensors*, 13(2013), No. 5, p. 6204.
[13] B.S. He and J.W. Li, A sensitive electrochemical sensor based on reduced graphene oxide/Fe_3O_4 nanorod composites for detection of nitrofurantoin and its metabolite, *Anal. Methods*, 11(2019), No. 11, p. 1427.
[14] T.K. Sari, F. Takahashi, J.Y. Jin, R. Zein, and E. Munaf, Electrochemical determination of chromium(VI) in river water with gold nanoparticles-graphene nanocomposites modified electrodes, *Anal. Sci.*, 34(2018), No. 2, p. 155.
[15] S.M. Zhu, J.J. Guo, J.P. Dong, Z.W. Cui, T. Lu, C.L. Zhu, D. Zhang, and J. Ma, Sonochemical fabrication of Fe_3O_4 nanoparticles on reduced graphene oxide for biosensors, *Ultrason. Sonochem.*, 20(2013), No. 3, p. 872.
[16] J.L. Zhang, H.J. Yang, G.X. Shen, P. Cheng, J.Y. Zhang, and S.W. Guo, Reduction of graphene oxide vial-ascorbic acid, *Chem. Commun.*, 46(2010), No. 7, p. 1112.
[17] K. Alamelu, V. Raja, L. Shiamala, and B.M. Jaffar Ali, Biphasic TiO_2 nanoparticles decorated graphene nanosheets for visible light driven photocatalytic degradation of organic dyes, *Appl. Surf. Sci.*, 430(2018), p. 145.
[18] Y.P. Zhang and C.X. Pan, TiO_2/graphene composite from thermal reaction of graphene oxide and its photocatalytic activity in visible light, *J. Mater. Sci.*, 46(2011), No. 8, p. 2622.
[19] Y. Zhao, D.L. Zhao, C.L. Chen, and X.K. Wang, Enhanced photo-reduction and removal of Cr(VI) on reduced graphene oxide decorated with TiO_2 nanoparticles, *J. Colloid Interface Sci.*, 405(2013), p. 211.
[20] E. Lee, D. Lee, J. Yoon, Y.L. Yin, Y.N. Lee, S. Uprety, Y.S. Yoon, and D.J. Kim, Enhanced gas-sensing performance of GO/TiO_2 composite by photocatalysis, *Sensors*, 18(2018), No. 10, art. No. 3334.
[21] Y. Haldorai, A. Rengaraj, C.H. Kwak, Y.S. Huh, and Y.K. Han, Fabrication of nano TiO_2@graphene composite: Reusable photocatalyst for hydrogen production, degradation of organic and inorganic pollutants, *Synth. Met.*, 198(2014), p. 10.
[22] M. Szabó, J. Kalmár, T. Ditrói, G. Bellér, G. Lente, N. Simic, and I. Fábián, Equilibria and kinetics of chromium(VI) speciation in aqueous solution − A comprehensive study from pH 2 to 11, *Inorg. Chim. Acta*, 472(2018), p. 295.